Journal of Structural Geology, Vol. 9, No. 5/6, pp. 691 to 704, 1987
Printed in Great Britain

0191-8141/87 $03.00 + 0.00

Rolling structures at large shear strain

JEAN VAN DEN DRIESSCHE and J.-P. BRUN

Laboratoire de Tectonique, U.E.R. Sciences Physiques de la Terre, Université Paris 7—I.P.G.P., 2, Pl Jussieu, 75230 Paris Cédex 05, France

(*Received* 7 *July* 1986; *accepted in revised form* 15 *February* 1987)

Abstract—At large shear strain, shear criteria are often obliterated or become ambiguous. From examination of both natural examples and experimental models we describe a new criterion called 'rolling structure', widely represented in sheared rocks. A typical rolling structure is composed of a rigid or competent object (e.g. porphyroclast, boudin, fossil, etc.) with two tails asymmetrically disposed around it. In most cases tails are of the same material as that of the rotating object, and result from strain softening and grain-size reduction at the object periphery, forming a mantle. Z and S asymmetries of rolling structures represent dextral and sinistral senses of shearing, respectively. Tails must not be confused with pressure shadows which usually present an opposite asymmetry for a given shear sense. Besides the determination of the sense of shear, the occurrence of these structures allows a minimum estimate of the strain intensity in strongly sheared rocks, since rolling structure length is proportional to shear strain.

INTRODUCTION

IN HIGHLY sheared rocks, determination of the sense of shear is often problematic. Features which can be used as shear criteria tend to develop from mechanical instabilities during shear deformation and are characterized by their asymmetry (Lagarde 1978, Burg *et al.* 1981, Simpson & Schmid 1983, Choukroune *et al.* 1987, Etchecopar & Malavieille, 1987). At large shear strain, the early developed asymmetrical structures tend to be modified or obliterated because of extreme flattening about the foliation plane (the $\lambda_1\lambda_2$ plane of finite strain). For example, *C*- and *S*-planes become parallel (Berthé *et al.* 1979a, Lister & Snoke 1984) and pressure shadows around clasts tend to lose their sigmoidal shape.

Later stage incremental features, such as asymmetric *C'*-shear bands may eventually develop during the progressive shearing and provide a useful additional shear criterion (Berthé *et al.* 1979b, Platt & Vissers 1980, Lister & Snoke 1984). Generally, however, it is difficult to determine the sense of shear at large finite shear strain. In this paper we discuss natural examples and present experimental models of rolling structures that are produced by the rotation of competent objects in a ductile matrix during large shearing deformation. These are called here *rolling structures* (Van Den Driessche 1986) and consist of a rigid object surrounded by asymmetrically rotated tails. The asymmetry of a rolling structure is seen to persist and amplify with the evolving deformation. Two end-member types can be separated, according to the nature and the origin of the tails. Firstly, in mylonites and ultramylonites feldspar porphyroclasts are progressively isolated in a grain-size reducing matrix. In this case, tail material is derived from the periphery of the clast. A second type of rolling structures results from the deformation of pre-existing planar features in the matrix that are rotated around rotating objects (boudins, pebbles, etc.).

Experimental models of such structures have been reproduced in simple-shear experiments, using Plasticine objects of rectangular shape embedded into a Newtonian silicone putty matrix. The experimentally produced structures are comparable to natural examples and verify similar previous theoretical and experimental work (Ghosh & Ramberg 1976, Shoneveld 1977, Fernandez *et al.* 1983, Lister & Williams 1983, Passchier & Simpson 1986, Passchier 1987). Experimental models (Van Den Driessche 1986) are also used to establish quantitative relationships between the geometry and dimensions of rolling structures and the finite strain.

ROLLING STRUCTURES IN MYLONITES

In mylonites, grain-size reduction is characteristic, so that porphyroclasts are preserved within a very fine-grained, strain-softened matrix best observed in $\lambda_1\lambda_3$ sections (i.e. parallel to the stretching lineation and perpendicular to the foliation). Granites from the Santa Catalina metamorphic core complex in southeastern Arizona are deformed by a crustal shear zone (work with G. Guerin, in preparation). Mylonites of this shear zone provide beautiful examples of rolling structures which are seen within a biotite-rich matrix. Metamorphism reaches the amphibolite facies. Rolling structures consist of feldspar porphyroclasts, surrounded by strongly elongated tails (Figs 1 and 4a). In most cases, the clast margins (mantles) appear highly strained. Tails are in continuity with the porphyroclast mantles and consist of dynamically recrystallized fine-grained feldspar (see also Passchier 1987). Total tail length can reach 10 times the mean diameter of the porphyroclast.

An ideal tail geometry can be described as follows (Van Den Driessche 1986): on both sides of the clast each tail displays a bulk sigmoidal shape, with an inflection point in the vicinity of the clast (Fig. 1). Beyond this

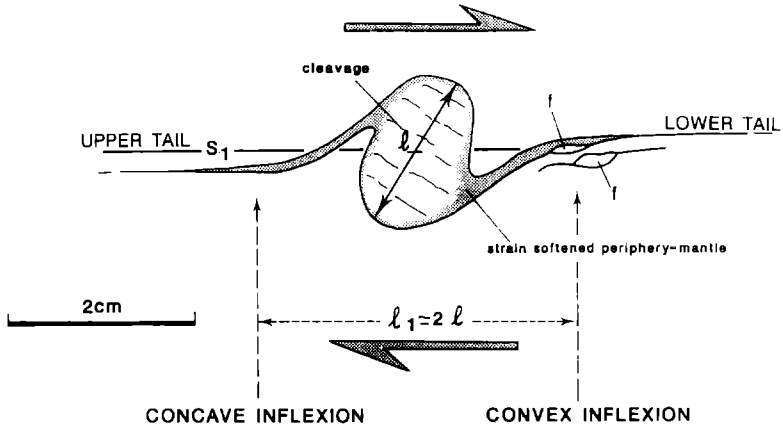

Fig. 1. Geometric characteristics of a typical rolling structure.

point, the tail curvature slowly dies out at a distance approximately equal to the clast long axis. Further away from the clast, the tail is rectilinear and concordant with the foliation. Between the inflection point and the clast, the tail is strongly curved around the clast margin. The two tails are termed upper and lower with respect to the mylonite foliation surface S whose continuation goes through the centre of the clast, thus defining a bulk asymmetry (Fig. 1). Near the inflection points, the curvature of the upper and lower tails are, respectively, concave and convex to the top. The occurrence of tail inflections can be used to indicate rolling of the clast.

The bulk asymmetry of the rolling structure is characteristic of the sense of shear: S and Z patterns correspond to sinistral and dextral sense of shear, respectively (Fig. 2). This is identical to the asymmetry of 'drag' folds developed in non-coaxial deformation. The short, often inverted, limb of such a fold corresponds to the position of the rigid clast within a rolling structure (Fig. 2). According to Lister & Williams (1983), both rolling structures and 'drag' folds in shear zones result from the vorticity partitioning of flow.

Tails of rolling structures can present tight appressed isoclonal folds, similar to fold patterns in the mylonitic matrix (Fig. 3). Examination of sections parallel to $\lambda_1\lambda_3$ and to $\lambda_2\lambda_3$ planes show that the axes of tail folds are subparallel to the stretching lineation, so that folds in $\lambda_1\lambda_3$ planes can be interpreted as passive folds (Donath & Parker 1964). This tends to demonstrate that in most cases tails deform with the ductile matrix which surrounds the clasts. In other words, tails of rolling structures act predominantly as passive markers during progressive shear deformation.

The following conclusions can be drawn from the natural examples in mylonites.

(1) Rolling structures result from the heterogeneous deformation of a rotating rigid object in a ductile matrix; tails are produced by grain-size reduction and softening of clast margins, producing mantles.

(2) S and Z patterns are characteristic of sinistral and dextral senses of shear, respectively.

(3) Passive folding of tails is indicative of a low viscosity contrast between the matrix and the tails.

(4) The observed tail geometry results from

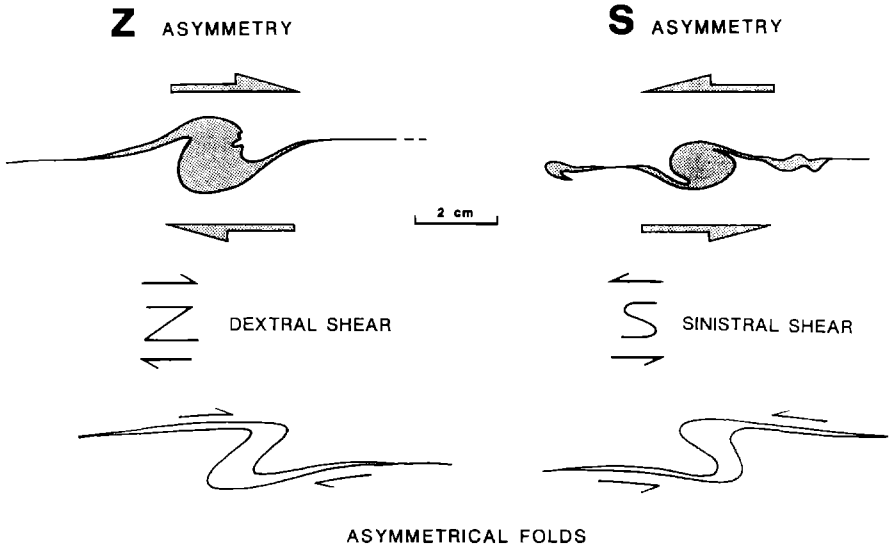

Fig. 2. S and Z asymmetry of rolling structures, allowing the determination of the sense of shear. Note comparison with 'drag' fold geometry in a shear regime.

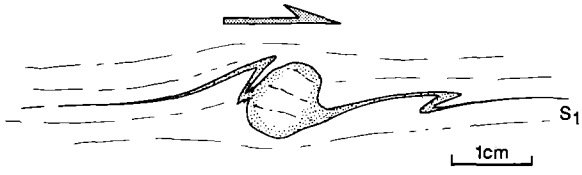

Fig. 3. Natural example of a folded tail to a rolling structure.

heterogeneous deformation of the matrix around the object. Once initiated, tails behave as passive markers during progressive shear deformation.

ASSOCIATED STRUCTURES

The concept of rolling structure as a shear criterion can be extended to any rigid object which rotates in a ductile matrix. Figure 4(b) shows an example of boudinage in a flysch series of alternating limestone and marl layers that has undergone a combination of layer-parallel shear and layer-parallel elongation (Merle & Brun 1984). The sense of shear is given by cleavage refraction. Boudins have been rotated in the sense of shear. The bedding parallel cleavage in marl layers is contorted around boudins in a fashion similar to the basic pattern of a rolling structure (Fig. 4b). The rolling structures are accentuated by drag of sedimentary planar markers around the rotating objects as modelled by Ghosh & Ramberg (1976). In this case no tails are produced from the periphery of the objects, but the resulting geometry is identical to rolling structures in mylonites.

EXPERIMENTAL MODELS

Procedure

To model rolling structures in shear zones, it has been assumed that the non-coaxial deformation in shear zones approaches progressive simple shear. Experiments in simple shear have therefore been carried out: (1) to investigate the progressive development of rolling structure around a rotating rigid object in a viscous matrix; and (2) to establish a possible quantitative relationship between the rolling structure dimensions and strain intensity.

The model consists of a rigid object embedded within a viscous matrix of silicone putty (Rhodorsil Gomme Special GS1R manufacturered by Rhône Poulenc, France). The rigid object is made of Plasticine and has a rectangular section with an axial ratio of 1:2 to simulate a common feldspar clast (Fig. 5). The silicone has an almost perfect linear dependence of stress upon strain rate, whereas Plasticine has a strongly non-linear dependence (see Cobbold & Quinquis 1980). During progressive shearing, the object rotates without internal deformation, while the silicone matrix flows. Several initial angles between the object long axis and the shear plane (α) of -45, 0, $+45$ and $+90°$ have been tested.

In a first series of experiments, the object is surrounded by a thin coloured silicone layer to simulate clast mantle (Fig. 5). This layering is prepared by mixing small amounts of finely powdered iron oxide (Fe_2O_3) with the silicone putty. The viscosity contrast between these thin coloured layers and the pure silicone matrix is very low and does not exceed 1.5:1.

Apparatus

The model (13 × 6.5 × 2 cm) is placed into a simple-shear machine (Fig. 6) which consists of two mobile lateral walls, which can be moved in opposite senses by two jacks. Displacement of the jacks is powered by a stepping motor controlled by microcomputer (Fig. 6).

The model lies over a basal plate which is coated with a liquid soap lubricant which minimizes friction against the lower surface of the model. The upper surface is free. The perfect adherence of the silicone putty to the lateral walls allows the shear couple to be integrally transmitted into the model. It is confined at its extremities by two silicone buffers of the same viscosity (Fig. 6).

The shear box is designed for attaining finite shear strains up to 25. To escape strong 3-D strain effects at the

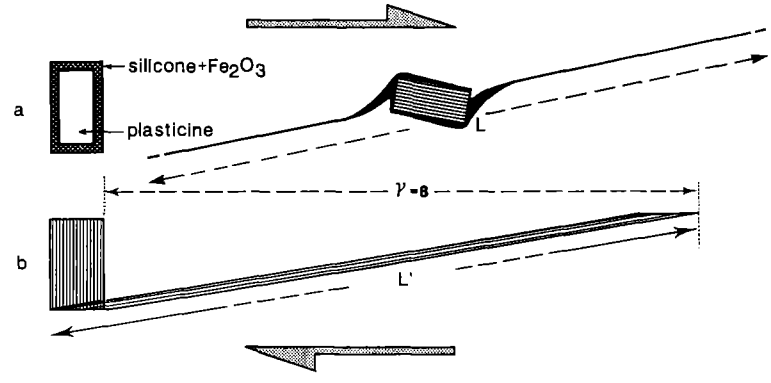

Fig. 5 (a). Rigid object made of Plasticine and surrounded by a thin coloured silicone layer, to simulate a clast mantle. During shearing, tails develop from the thin coloured silicone layer, as shown systematically. (b) Deformation of a passive object of the same dimensions as the object in (a). Note that the rolling structure length in (a) is nearly equal to the maximum length of the deformed object in (b).

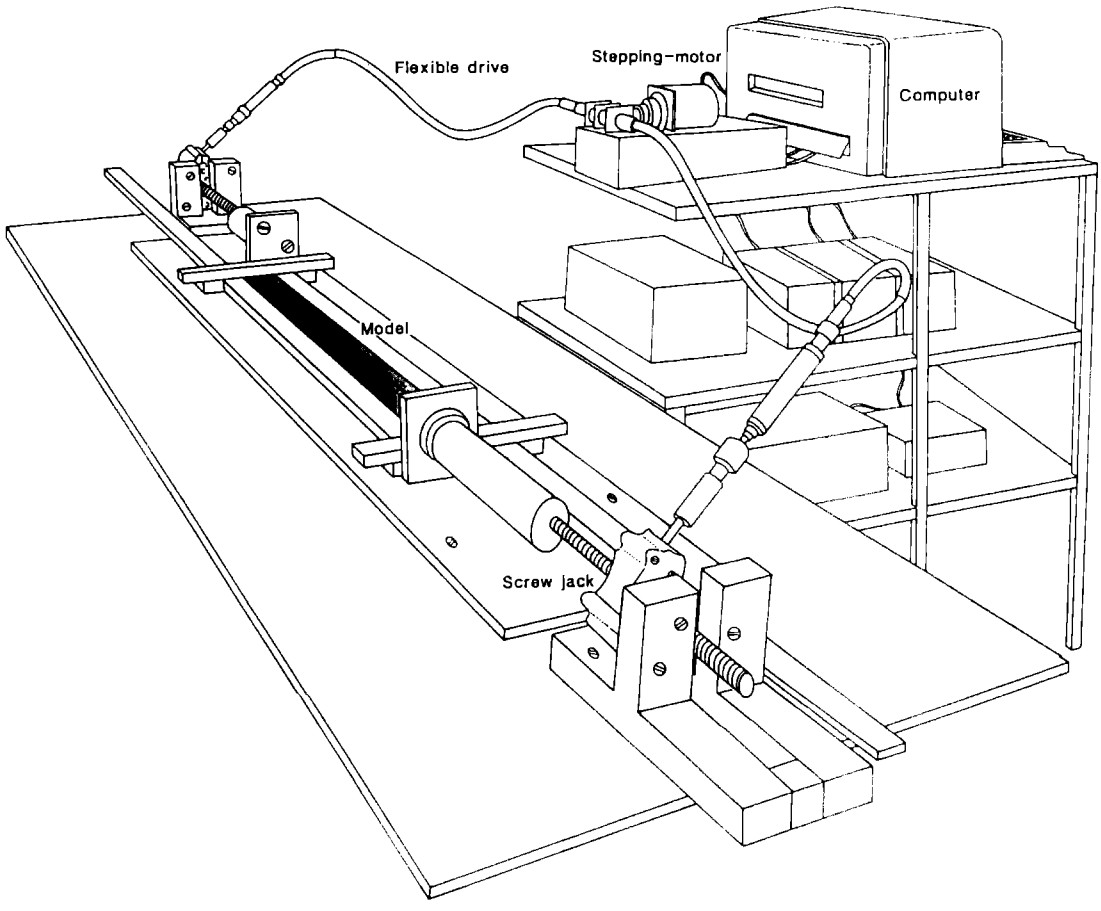

Fig. 6. Shear apparatus with electronic control. The shear machine is seen at the final stage of an experiment. The sense of shear is dextral.

free surface, low shear strain rates were imposed ($\dot{\gamma} = 10^{-3} - 10^{-4}\,s^{-1}$).

Visual display

Once the model is placed into the shear box, a strain grid is printed on the free surface. The most convenient grid is one of small regularly spaced circles which deform into strain ellipses. This allows observation of evolving progressive strain during the experiments. The bulk 3-D finite strain state of modelled rolling structures was observed by dissecting the model after freezing to −30°C, to limit any induced internal deformation due to cutting.

RESULTS

Geometric observations

Figures 7 and 8 show models which have undergone different finite shear strains. Clast–tail systems analogous to natural rolling structures have been obtained for any starting orientation (α) of the object. Finite shear strain values γ vary from 7 to 13.

As in the natural examples, the models show the following characteristics: (1) concave and convex inflections of the upper and lower tails, respectively; (2) a Z pattern, resulting from the imposed dextral shear.

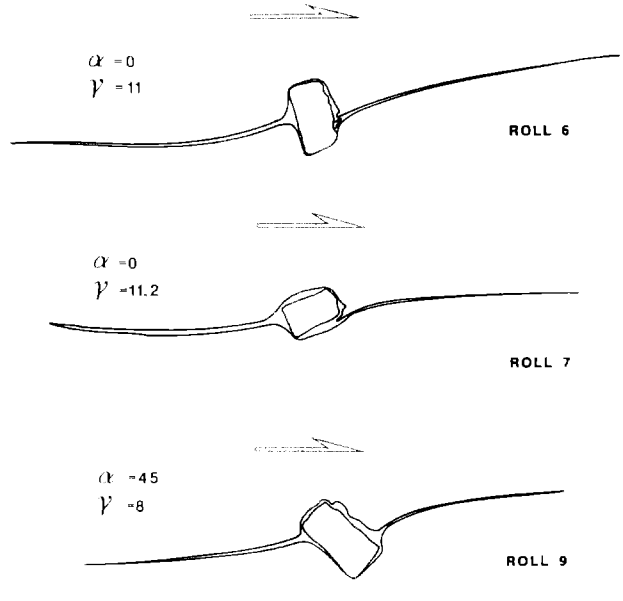

Fig. 7. Examples of modelled rolling structures. α is the starting angle between the object long axis and the shear plane. In experiments 6 and 7 the objects had the same starting position and have undergone a similar shear strain of ca 11. The object in 7 has rotated much more because the viscosity of the matrix silicone putty was lowered by heating from flood-lights. In experiment 9 (Fig. 8a) the starting angle (α) was at −45° clockwise from the shear plane.

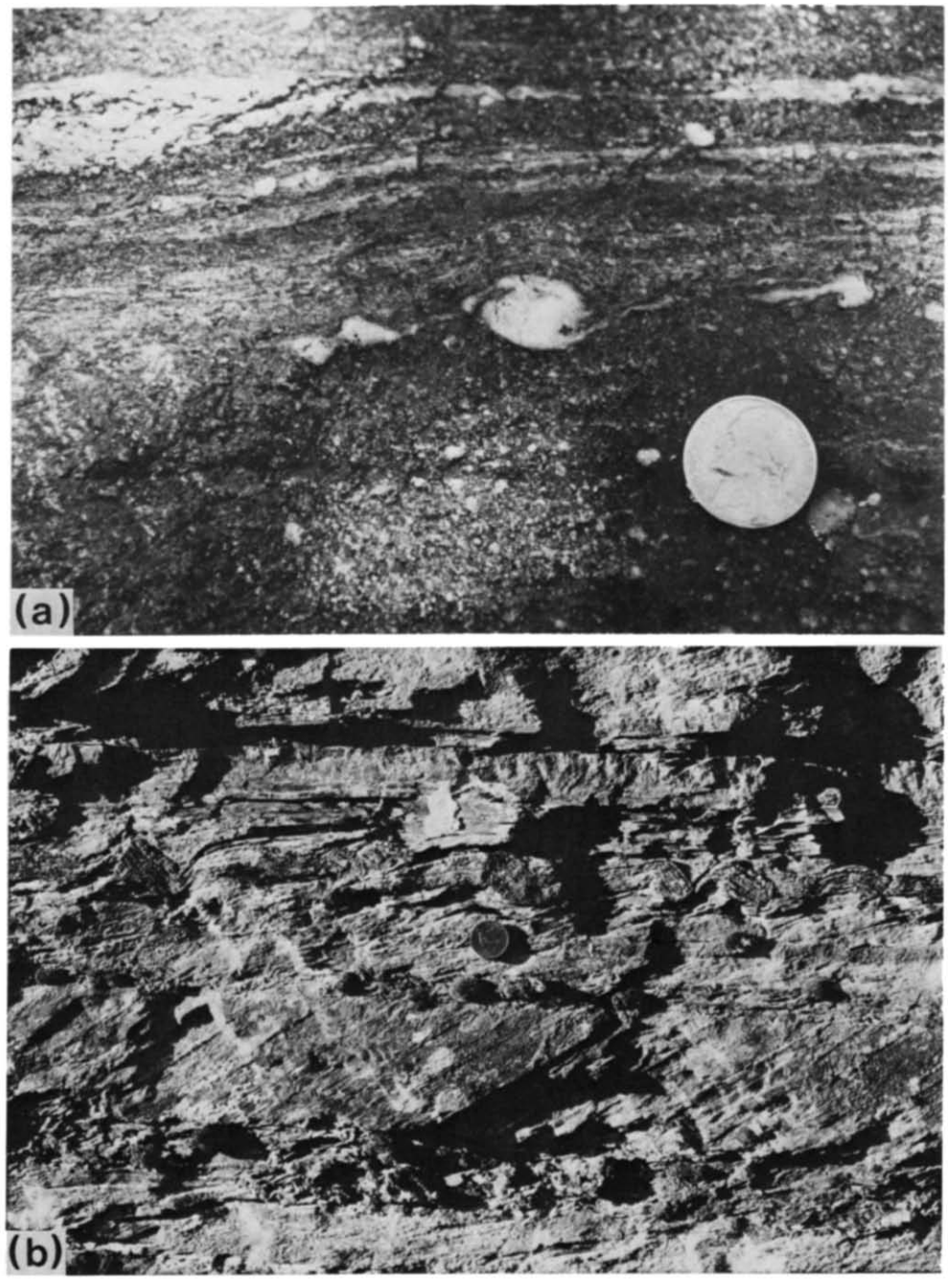

Fig. 4 (a). Example of rolling structures developed from feldspar porphyroclasts (Santa Catalina metamorphic core complex, southeastern Arizona). (b). Rolling structures developed from a boudinaged competent limestone layer in a flysch series of the Parpaillon Nappe (French Alps).

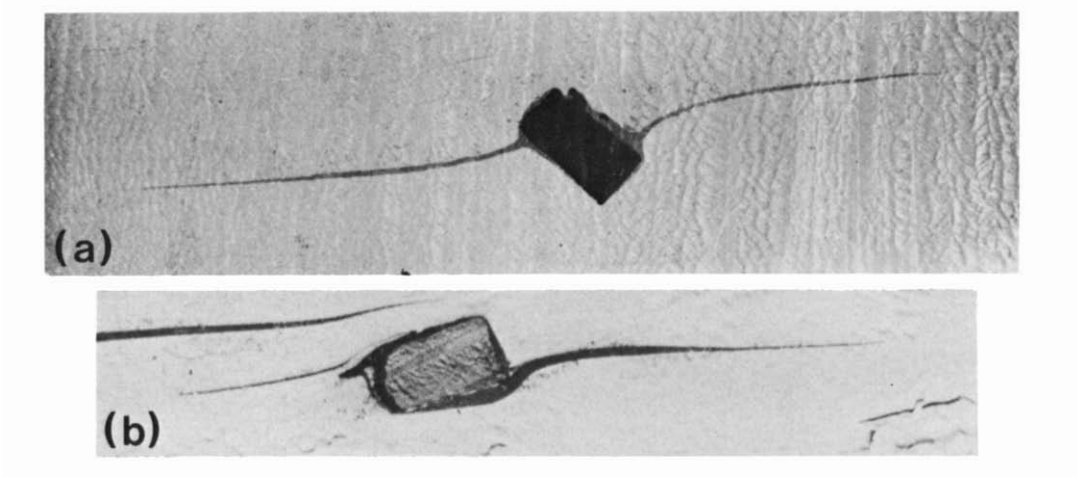

Fig. 8 (a). Experiment 'roll 9' with starting angle $\alpha = -45°$ and $\gamma = 8$ (see Fig. 7a). (b) Experimental rolling structure wi folded tail. Compare the geometry with the natural example in Fig. 3.

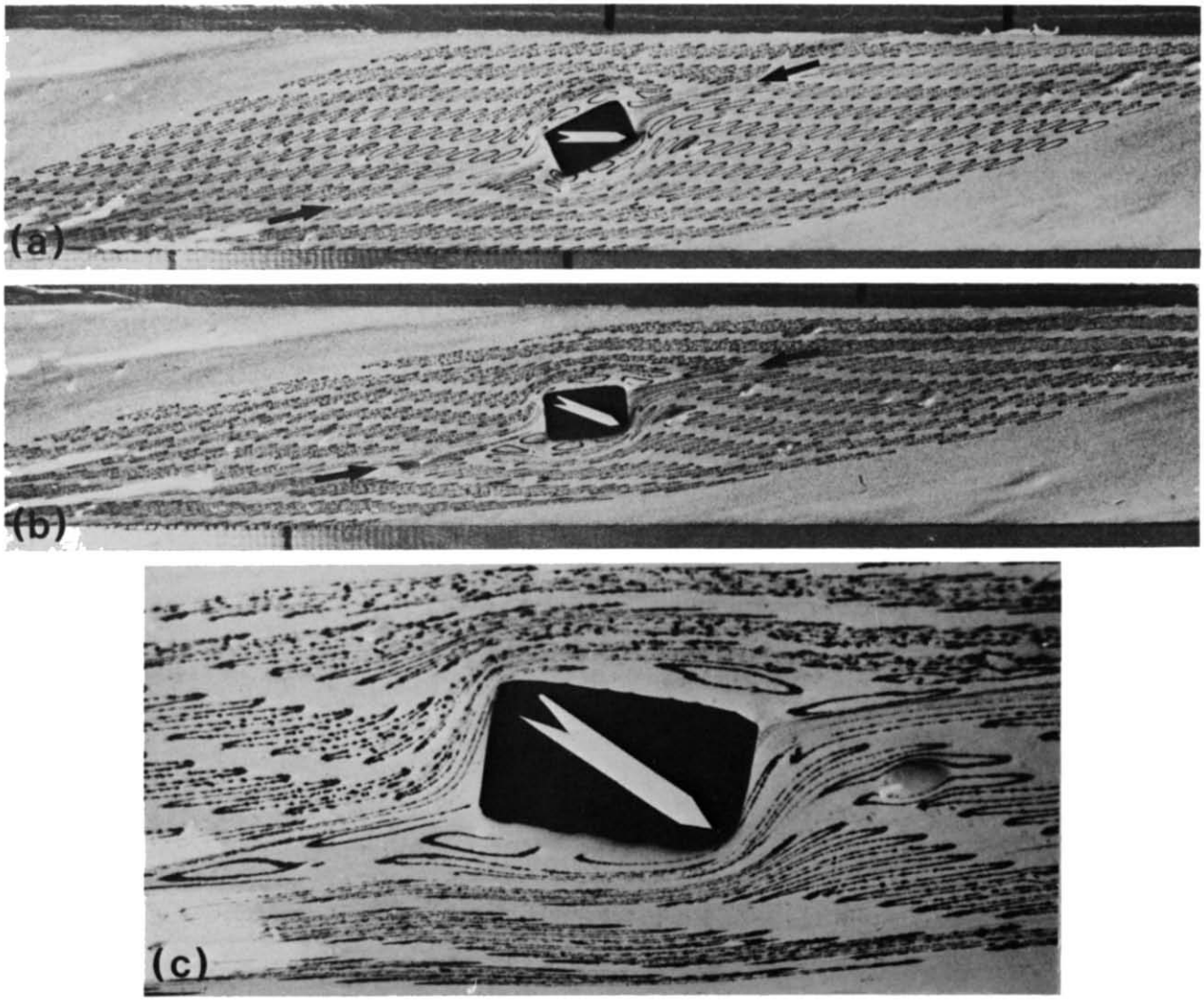

Fig. 9. Evolution of strain at the free surface. Note the development of passive isoclinal folds in the matrix in the vicinity of the right-upper and left-lower corners of the object. Curve envelopes of strain ellipses in (a) and (b) have been traced on Fig. 11(b) & (c), respectively. (c) Detail of finite strain state γ (bulk) = 9 immediately adjacent to the object. Note the extreme elongation of ellipses near the object upper-left and lower-right corners. Conversely, near the upper-right and lower-left some ellipses seem to have undeformed.

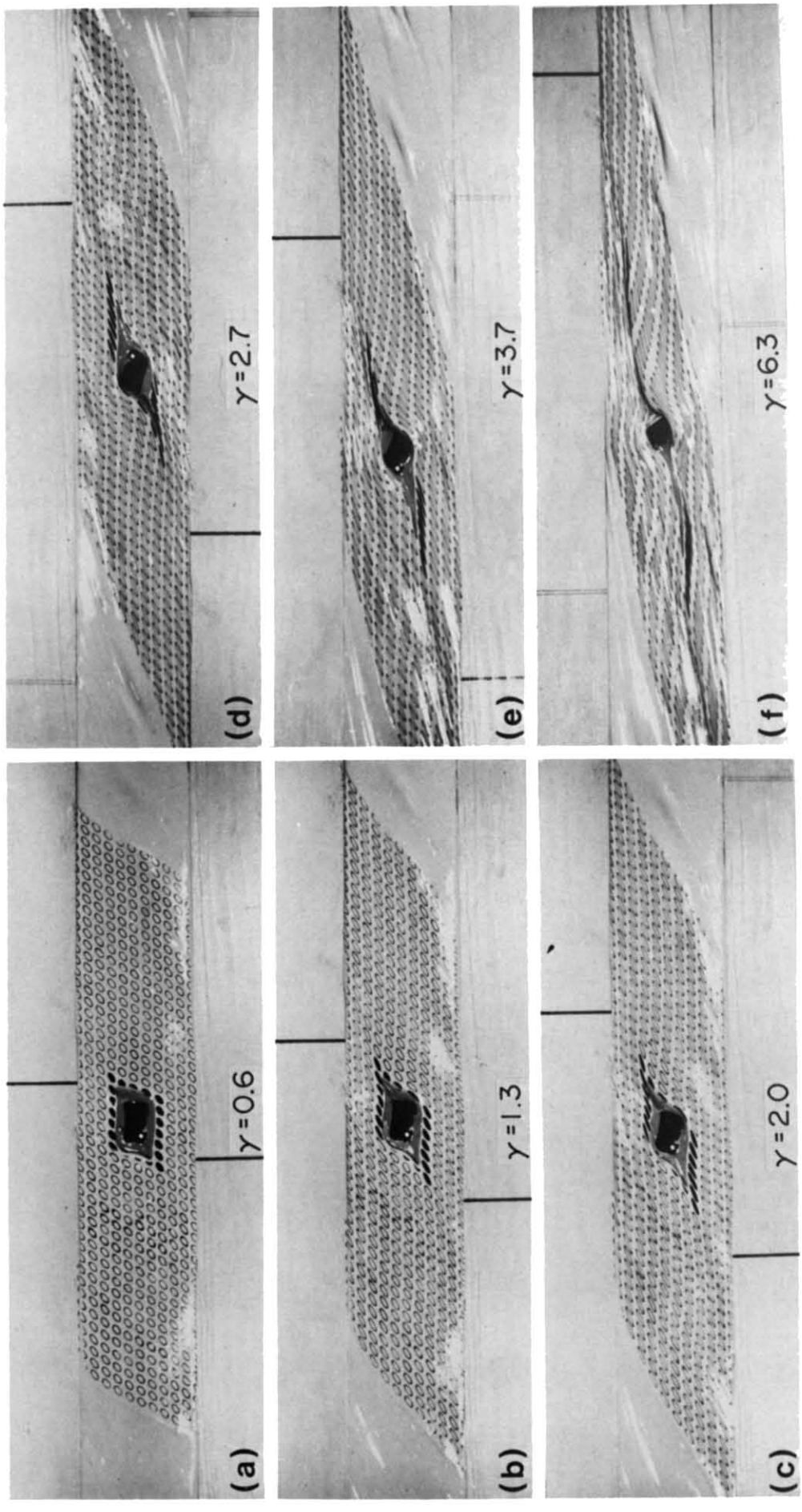

Fig. 12. Progressive development of rolling structure tails at the free surface (experiment roll 7).

Geometrical similarities between modelled and natural rolling structures confirm that tails behave essentially as passive markers of the heterogeneous deformation induced by rigid clast rotation in a ductile matrix. Some models show folded tails markedly resembling the natural examples (Fig. 8b). The occurrence of folded tails in the models depends on the viscosity contrast between the matrix silicone and the thin coloured silicone layer. This contrast can be accentuated by mixing larger amounts of powdered iron oxide which makes the silicone putty more competent. The viscosity contrast, though low (1.5/1), may act as a weak mechanical instability responsible for folding of the tails. However, models in which the viscosity contrast between the silicone matrix and the silicone mantle is very low can show either folded or non-folded tails. When folds occur, they are extremely isoclinal (Fig. 8b) and result from the kinematic amplification of geometrical perturbations during tail development (Cobbold & Quinquis 1980). A significant relationship exists between tail length and strain intensity. This is described in more detail below.

Progressive deformation at the free surface (Fig 9)

In these experiments no coloured silicone layer has been added around the object. The grid circles are progressively deformed into ellipses, indicating the strain intensity. Rotational velocity of the object is not constant during progressive simple shear. The curve giving the value of α as a function of γ is similar to that obtained by Fernandez *et al.* (1983) (Fig. 10).

In Fig. 11, curved envelopes of strain ellipses have been traced to emphasize the strain pattern induced by the rigid body rotation in passive layers. At the first stages, layers are warped adjacent to the upper and lower faces of the object. Warping progressively evolves into strongly appressed isoclinal folds (Figs. 9 and 11). Note that the strain pattern in the matrix is asymmetrical with respect to the object. Folds in the matrix developed in the same way for any initial object position. On both sides of the object, the short limbs of folds define an oblique band parallel to the λ_1 axis away from the object (Figs. 9 and 11). At first sight, this band appears as a shear zone, but strain gradients and principal strain trajectories, displayed by the shape of ellipses, show that it is certainly not a shear zone (compare with Ramsay & Graham 1970, and Ramsay 1980). It can be seen: (1) that zones of equivalent strain intensity surround the rigid object and cross-cut the band; and (2) that the band is parallel to the λ_1 axis of strain ellipses where the layer boundaries are not disturbed (i.e. away from the object, in homogeneous simple shear). So this band results from the passive amplification of a fold induced by unsteady-state flow around the object. This process can be compared with one described and theorized by Hudleston (1976) and experimentally modelled by Brun & Merle (1987). Small-scale natural examples of such a passive folding process have been described by Berthe & Brun (1980, fig. 4). In some natural examples, oblique bands connected with clasts have been interpreted as shear bands but may in fact have resulted from the process described above. Immediately adjacent to the object, strain appears to be extremely heterogeneous (Fig. 9c). The centres of ellipses are strongly displaced from their initial positions adjacent to the object boundaries. The long axes of some reference ellipses are warped and can reach 9 times the initial circle radius. Stretching of these ellipses is higher than in zones which are not disturbed by the object rotation and only affected by imposed simple shear. Strain intensity in the matrix is thus high adjacent to the object.

In a second series of experiments, the object is surrounded by a thin coloured layer. Figure 12 shows how tails developed with evolving strain marked by the deformed grid at the free surface of the model. For any initial position of the object, tails initiate in the principal extension direction of incremental strain (Fig. 12). Away from the object, tails are stretched in the direction of bulk finite strain (λ_1) and show a rectilinear pattern. Near the object, tails are warped by object rotation, resulting in the characteristic geometry of rolling structures (Figs. 7 and 8).

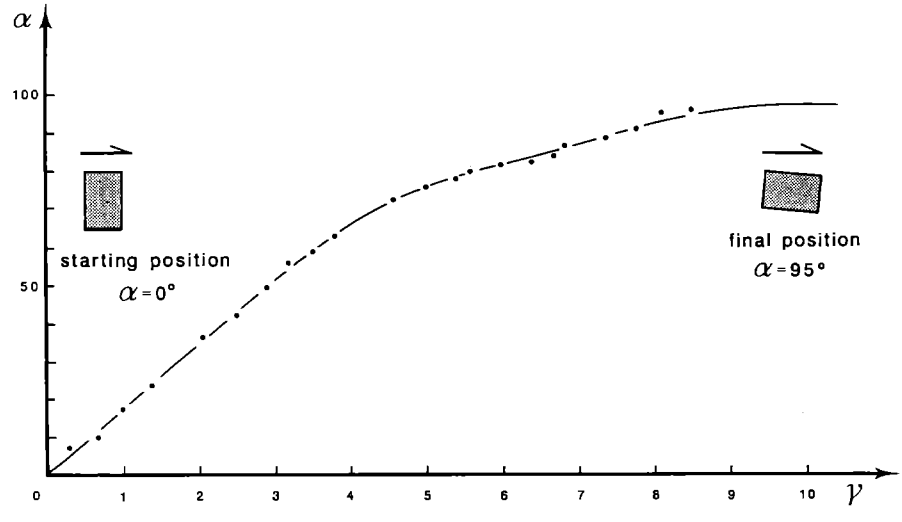

Fig. 10. Variations of the angular rotation of a rigid object vs shear strain.

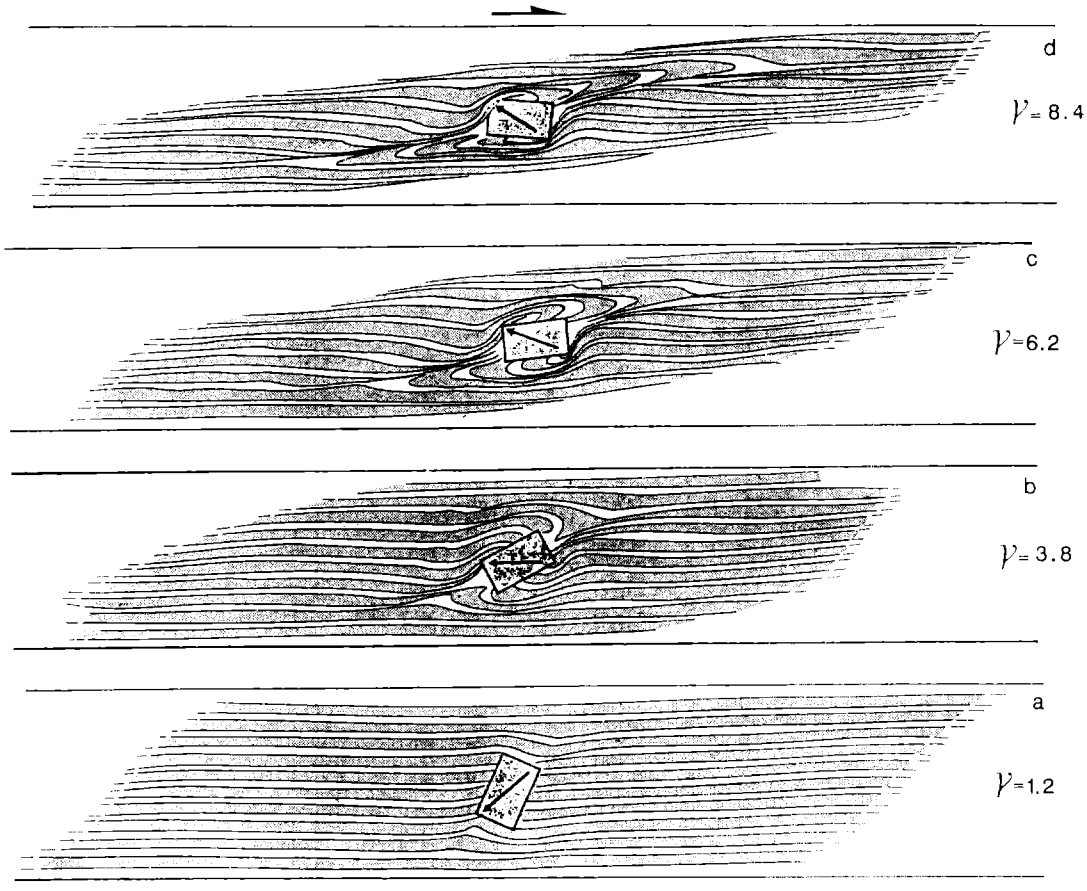

Fig. 11. 'Layers' of strain ellipses demonstrate progressive passive folding in the matrix for increasing simple-shear deformation.

Relationships between rolling structure length and finite strain

Experiments show that rolling structure length is a function of: (1) strain intensity; (2) axial ratio of the thin silicone layer surrounded object; and (3) the starting orientation of the object (Fig. 14). More precisely, rolling structure length L is proportional to a passive stretched segment of line d that makes an initial angle of 45° with the shear plane and passes through the centre of the object (Fig. 14a). If a and b are, respectively, the long and short object axes, the initial length of this segment of line (d) is equal to $b \div \sin 45°$, $b \div \sin 45°$, a and b for objects with initial starting orientations (α) of 90, 0, +45 and −45°, respectively. Rolling structure lengths (L) have been graphically predicted in Fig. 14(a) for a γ value of 10, an initial object axial ratio of two and four different object starting orientations. Figure 14(b) and (c) shows the good fit between these predictions and the experimental data.

Rolling structure length can also be theoretically predicted for large finite shear strains. At large shear strain ($\gamma > 5$), the γ value approaches the value of principal stretch $\lambda_1^{1/2}$, so that $\lambda_1^{1/2} \cong \gamma$ (see Ramsay 1967, figs. 3–21). Because tails develop parallel to the incremental strain axis during the first stage of the progressive shearing in models, the final length of the rolling structure (L) is almost equal to the $\lambda_1^{1/2}$ value of finite strain (assuming that the initial length of the segment of line at 45° to the shear plane is equal to 1). In practical terms, shear strain can be obtained in the models from the ratio between the total length of the rolling structure (L) and the length of the initial segment of line (d) so that $\gamma = L/d$.

DISCUSSION

From field evidence described in this paper, we consider that rolling structure tails behave almost passively in the surrounding matrix. Previous studies of rolling structures (Van Den Driessche 1986, Passchier 1987) have proposed that the tail material comes from clast mantle, and that grain-size reduction in this mantle results from strain softening (Passchier 1987). Therefore, the rolling structures considered here cannot be equivalent to pressure-shadow clast systems in which tails grow onto the clast. Thus, the experiments were designed to model a purely passive process. In the models, the thin coloured silicone layer which surrounds the rigid object, represents the softened mantle observed in natural clasts (Van Den Driessche 1986, Passchier 1987). Models show that strain intensity is much higher in the matrix adjacent to the object than away from it. Although no simple relation can be postulated between strain intensity and strain softening, this process would seem to have been activated during the

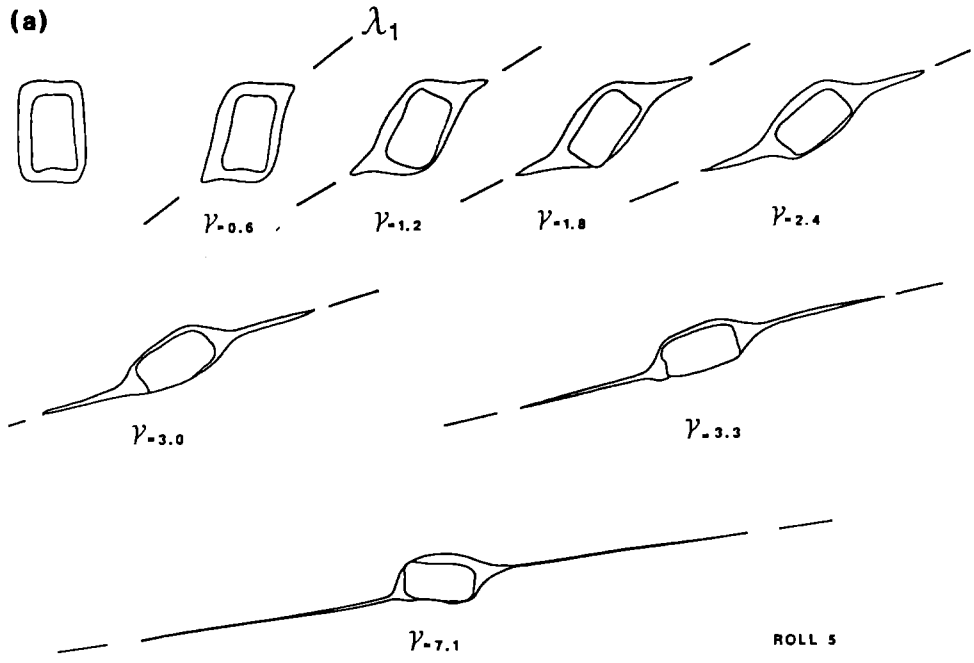
(a)
λ_1
$\gamma_{=0.6}$
$\gamma_{=1.2}$
$\gamma_{=1.8}$
$\gamma_{=2.4}$
$\gamma_{=3.0}$
$\gamma_{=3.3}$
$\gamma_{=7.1}$
ROLL 5

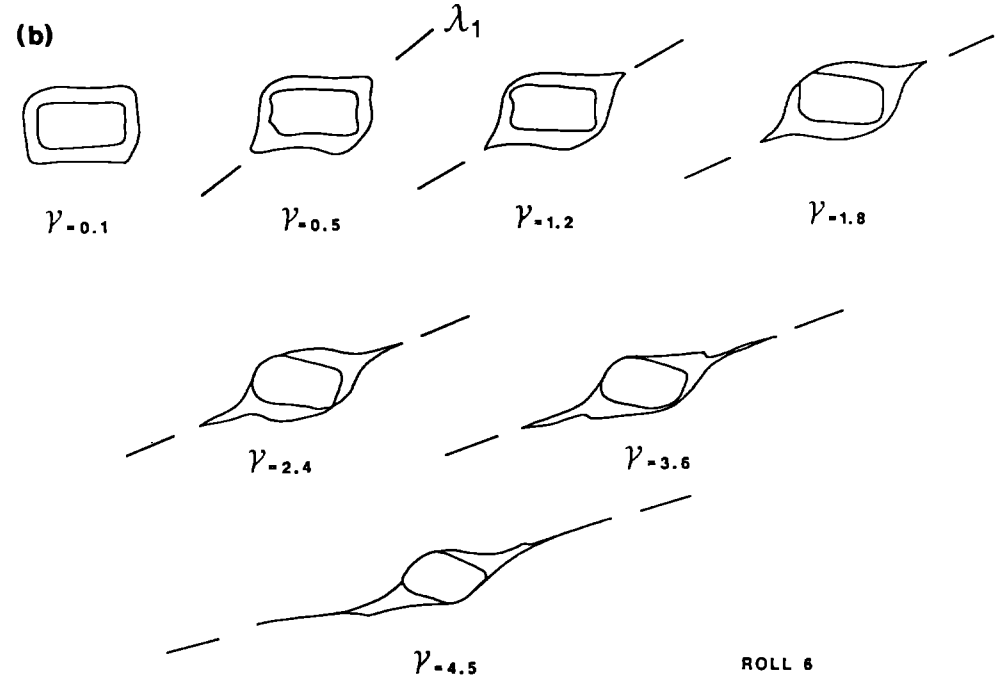
(b)
λ_1
$\gamma_{=0.1}$
$\gamma_{=0.5}$
$\gamma_{=1.2}$
$\gamma_{=1.8}$
$\gamma_{=2.4}$
$\gamma_{=3.6}$
$\gamma_{=4.5}$
ROLL 6

Fig. 13(a) & (b).

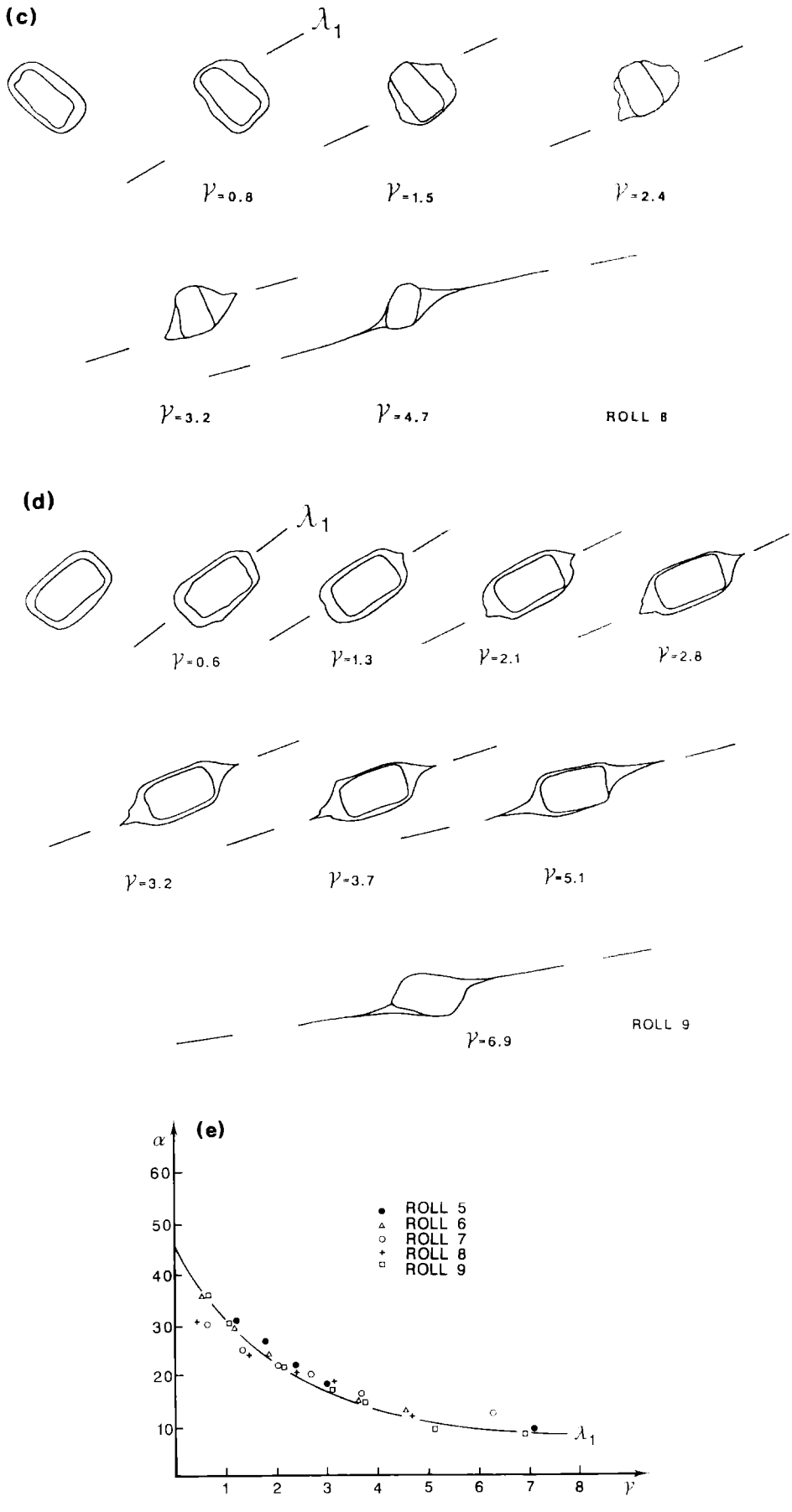

Fig. 13 (a)–(d). Progressive development of tails for different starting positions (α = 90, 0, −45, +45 degrees, clockwise rotation). (e) Graph of α values (angle between the tail orientation and the shear plane) vs shear strain (γ) for the experiments with different starting positions. Note the very good fit between the theoretical curve of λ_1 axis orientation vs shear strain and experimental data. It shows that rolling structure tails develop in the λ_1 direction for any starting positions of the object.

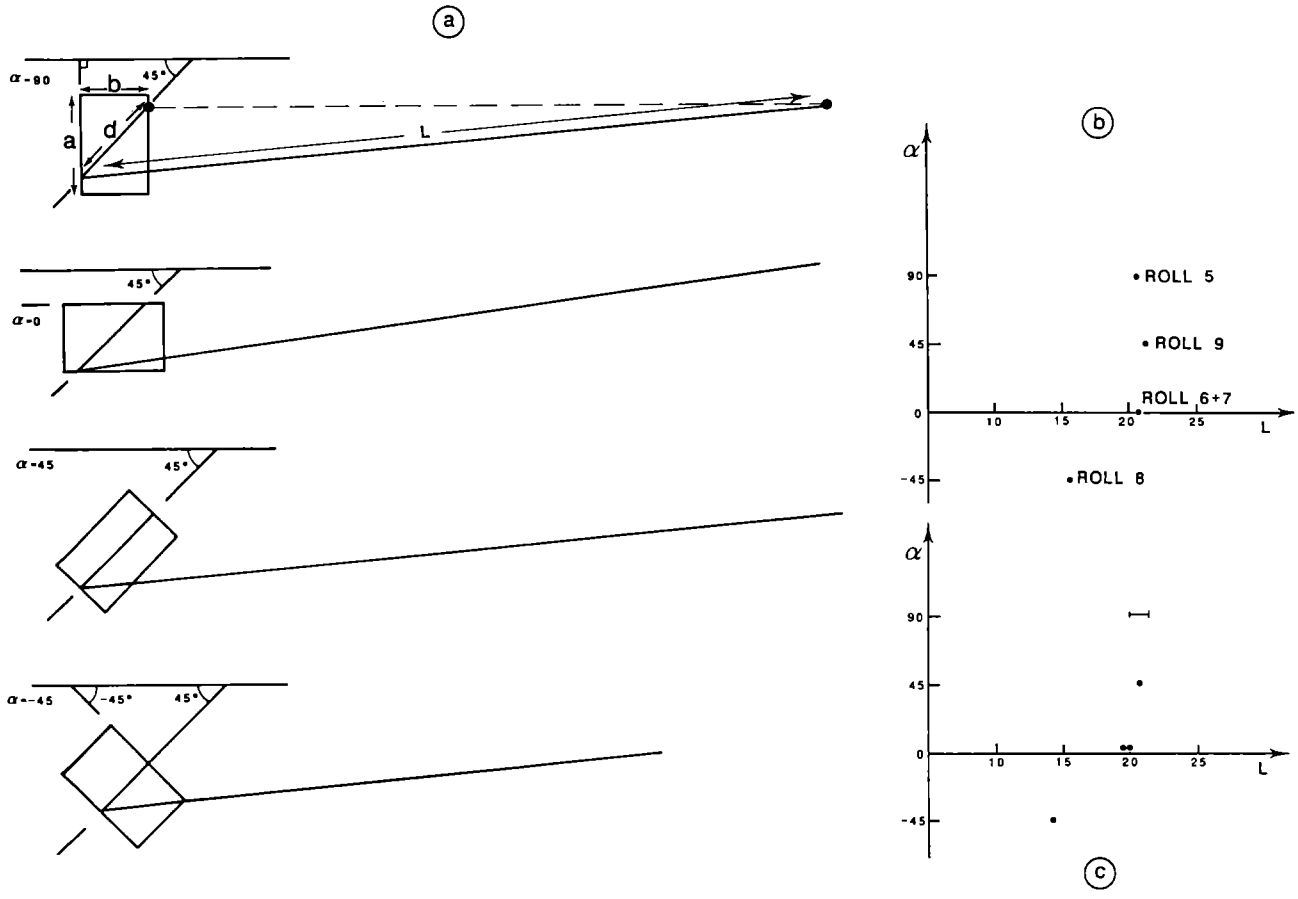

Fig. 14. Relationships between rolling structure length and shear strain. (a) Graphical prediction of rolling structures length, L, with respect to the object starting orientation (α) for a shear strain of 10 and an object axial ratio of 2 (see text for explanation). (b) and (c) Predicted lengths and experimental data, respectively, vs starting orientation (α) for $\gamma = 10$.

rotation of the clast. So the modelled rolling structures correspond to a relatively advanced stage of progressive shear in natural examples. As demonstrated by experiments, and assuming simple-shear deformation in mylonites, a minimum shear strain estimate can be deduced from the ratio between clast mean dimension and rolling structure length, especially when the axial ratio is equal to 1. For natural examples, such a relationship is applicable because tail initiation requires high strain intensity. Shear strain will be an underestimate because clast mantle thickness is difficult or impossible to determine, so that object (clast + mantle) dimensions will be always minimized. Nevertheless the relation that exists between rolling structure length and shear strain can be a very useful method of estimating strain intensity in mylonites, particularly where traditional methods cannot be used.

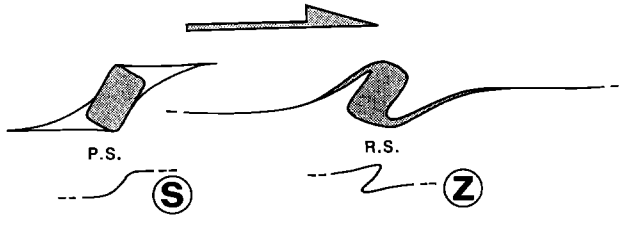

Fig. 15. Comparison between pressure shadow asymmetry and rolling structure asymmetry.

The warping of tails around clasts is an important feature that allows the determination of the sense of clast rotation, and thus the sense of shear. This characteristic is not restricted to the rolling structures described above, but can also occur in pressure-shadow clast systems if the ductility contrast between the tails and matrix is sufficiently low. Note that the asymmetry of pressure-shadows clast systems is the inverse of the rolling structure asymmetry (Van Den Driessche 1986, Passchier & Simpson 1986) (Fig. 15). The rolling effect in pressure-shadow clast systems may explain some apparent contradictions in shear-sense determinations from the same sample (see, for example Quinquis & Choukroune 1985, p. 415).

CONCLUSIONS

At large shear strains, rolling structures are very useful shear criteria. Natural examples and experimental models provide the following conclusions.

(1) Rolling structures result from strain patterns developed by rotating rigid clasts in a ductile matrix. A high rheological contrast between the clast and the matrix allows the shear induced vorticity in the matrix to be converted into spin in the clast.

(2) S and Z asymmetry of rolling structures indicate sinistral and dextral senses of shear, respectively.

(3) Rolling structure tails act predominantly as passive markers during progressive shearing.

(4) Tail geometry results from strain in the matrix which in turn results from rigid body rotation of the clasts.

(5) Development of rolling structures allows an evaluation of the rheological behaviour of rocks in shear zones.

(6) Rolling structure length is proportional to strain intensity; a quantitative estimate of finite shear strain can be obtained from the ratio of rolling structure length and clast mean dimension.

Acknowledgements—We gratefully acknowledge J. P. Burg, S. H. Treagus and two anonymous referees for critically reading the manuscript and suggesting improvements, and J. Dyon for promptly drawing all the figures. Experiments could not have been realized without the assistance of P. Allemand, J. Ballard, M. O. Beslier and moral support of J. Dyon.

REFERENCES

Berthé, D., Choukroune, P. & Jegouzo, P. 1979a. Orthogneiss mylonite and non coaxial deformation of granite: the example of the South Armorican Shear Zone. *J. Struct. Geol.* **1**, 31–42.

Berthé, D., Choukroune, P. & Gapais, D. 1979b. Orientations préférentielles du quartz et orthogneissification progressive en régime cisaillant: l'example du cisaillement sud armoricain. *Bull. Minéral.* **102**, 265–272.

Berthé, D. & Brun, J. P. 1980. Evolution of folds during progressive shear in the South Armorican Shear Zone, France. *J. Struct. Geol.* **2**, 127–133.

Brun, J. P. & Merle, O. 1987. Experiments on folding in spreading-gliding nappes. *Tectonophysics* In review.

Burg, J. P., Iglesias, M., Laurent, P., Matte, P. and Ribeiro, A. 1981. Variscan intracontinental deformation: the Coimbra–Cordoba shear zone (SW Iberian Peninsula). *Tectonophysics* **78**, 161–177.

Choukroune, P., Gapais, D. & Merle, O. 1987. Shear criteria: and structural symmetry. *J. Struct. Geol.* **9**, 525–530.

Donath, F. A. and Parker, R. B. 1964. Folds and folding. *Bull. geol. Soc. Am.* **75**, 45–62.

Cobbold, P. R. & Quinquis, H. 1980. Development of sheath folds in shear regime. *J. Struct. Geol.* **2**, 119–126.

Etchecopar, A. & Malavieille, J. 1987. Computer models of pressure shadows: a method for strain measurement and shear-sense determination. *J. Struct. Geol.* **9**, 667–677.

Fernandez, A., Feybesse, J. L. & Mezure, J. P. 1983. Theoretical and experimental study of fabrics developed by different shaped markers in two-dimensional simple shear. *Bull. Soc. géol. Fr.* **25**, 319–326.

Ghosh, S. K. & Ramberg, H. 1976. Reorientation of inclusions by a combination of pure shear and simple shear. *Tectonophysics* **34**, 1–70.

Hudleston, P. J. 1976. Recumbent folding in the base of the Barnes ice cap, Baffin Island, northwest Territories, Canada. *Bull. geol. Soc. Am.* **87**, 1684–1692.

Lagarde, J. L. 1978. La déformation des roches dans les domaines a schistosité horizontale. Application à la nappe du Canigou—Roc de France (Pyrénées Orientales) et au complexe cristallophyllien de Champtoceaux (Massif Armoricain). Unpublished thèse 3 cycle, Université de Rennes.

Lister, G. S. & Williams, P. F. 1983. The partitioning of deformation in flowing rock masses. *Tectonophysics* **92**, 1–33.

Lister, G. S. & Snoke, A. W. 1984. *S–C* mylonites. *J. Struct. Geol.* **6**, 617–638.

Merle, O. & Brun, J. P. 1984. The curved translation path of the Parpaillon nappe (French Alps). *J. Struct. Geol.* **6**, 711–719.

Passchier, C. W. & Simpson, C. 1986. Porphyroclast systems as kinematic indicators. *J. Struct. Geol.* **8**, 831–843.

Passchier, C. W. 1987. Stable position of rigid objects in non-coaxial flow—a study in vorticity analysis. *J. Struct. Geol.* **9**, 679–690.

Platt, J. P. & Vissers, R. M. 1980. Extensional structures in anisotropic rocks. *J. Struct. Geol.* **2**, 397–410.

Ramsay, J. G. 1980. Shear zone geometry: a review. *J. Struct. Geol.* **2**, 83–99.

Ramsay, J. G. & Graham, R. H. 1970. Strain variations in shear belts. *Can. J. Earth Sci.* **7**, 786–813.

Shoneveld, C. 1977. A study of some typical inclusion patterns in strongly para-crystalline rotated garnets. *Tectonophysics* **39**, 453–471.

Simpson, C. & Schmid, S. 1983. An evaluation of criteria to deduce the sense of movements in sheared rocks. *Bull. geol. Soc. Am.* **94**, 1281–1288.

Van Den Driessche J. 1986. Structures d'enroulement et sens de cisaillement. *C. r. Acad. Sci., Paris* **303**, 413–418.

SHEAR CRITERIA IN ROCKS

Section V:

Petrofabrics